

fabricated antenna. As can be seen from Figure 8, a good agreement between the simulated and measured results is obtained. However, there are some discrepancies between them that can be attributed SMA connectors, measured environmental effects and fabrication tolerances. It is observed from Figure 8 that the fabricated antenna has UWB range of 2.85–12 GHz along with two notch bands of frequencies 3.5 and 5.5 GHz.

Figure 9 shows measured radiation pattern in H -plane (x - y plane) and E -plane (y - z plane) at 4.3 and 6.6 GHz. It can be observed that the radiation pattern of H -plane is nearly omnidirectional for both the frequencies. The E -plane pattern is bidirectional in nature. The gain of the proposed UWB antenna with and without notched bands are shown in Figure 10. The gain of UWB antenna is nearly constant (3.6–5.6 dBi) in the entire UWB range. However, with the introduction of band notch elements at WiMAX and WLAN frequencies, the gain becomes negative which shows the good band-notch performance of UWB antenna.

4. CONCLUSION

In this letter, a modified circular monopole UWB antenna with noninteracting dual band notch characteristics is realized. The band notch characteristics are obtained by an elliptical slot in the radiating patch and a G-shaped slot in the ground plane under the feed line. A relevant mathematical expression for the length of half wavelength elliptical slot has been presented in terms of notch band frequency, slot width and the substrate thickness. The proposed UWB antenna can operate from 2.85 to 12 GHz with two rejection bands at 3.5 and 5.5 GHz. The proposed antenna is fabricated on low cost FR4 substrate and measured. The designed antenna has a small size of $25 \times 20 \text{ mm}^2$. The radiation pattern of the propose antenna is nearly omnidirectional throughout UWB frequency range.

REFERENCES

1. First Report and Order, Federal Communications Commission revision of Part 15 of the commission's rules regarding ultra-wideband transmission systems from 3.1 to 10.6 GHz, Federal Communications Commission, Washington, DC, 2002.
2. M. Ojaroudi, G. Ghanbari, N. Ojaroudi, and C. Ghobadi, Small square monopole antenna for UWB applications with variable frequency band-notch function, *IEEE Antennas Wireless Propag Lett* 8 (2009), 1061–1064.
3. S.J. Hong, J.W. Shin, H. Park, and J.H. Choi, Analysis of the band-stop techniques for ultrawideband antenna, *Microwave Opt Tech Lett* 49 (2007), 1058–1062.
4. X.L. Bao and M.J. Ammann, Printed band-reject UWB antenna with H-shaped slot, International Workshop on Antenna Technology: Small and Smart Antennas Metamaterials and Applications, Cambridge, 2007, pp. 319–322.
5. Q. Chu and Y. Yang, A compact ultrawideband antenna with 3.4/5.5 GHz dual band-notched characteristics, *IEEE Trans Antennas Propag* 56 (2008), 3637–3644.
6. Y. Zhang, W. Hong, C. Yu, Z.Q. Kuai, Y.D. Don, and J.Y. Zhou, Planar ultrawideband antennas with multiple notched bands based on etched slots on the patch and/or split ring resonators on the feed line, *IEEE Trans Antennas Propag* 56 (2008), 3063–3068.
7. M.C. Tang, S. Xiao, T. Deng, D. Wang, J. Guan; B. Wang; G.D. Ge, Compact UWB Antenna With Multiple Band-Notches for WiMAX and WLAN, *IEEE Trans Antennas Propag* 59 (2011), 1372–1376.
8. R. Janaswamy and D.H. Schaubert, Characteristic impedance of a wide slotline on low-permittivity substrates, *IEEE Trans Microwave Theory Techn* 34 (1986), 900–902.

COMPACT DUAL-ANTENNA WITH π -SHAPE GROUNDED STRIP FOR ENHANCED BANDWIDTH AND DECREASED COUPLING FOR LTE TABLET COMPUTER APPLICATION

Kin-Lu Wong and Po-Wei Lin

Department of Electrical Engineering, National Sun Yat-sen University, Kaohsiung 80424, Taiwan; Corresponding author: wongkl@ema.ee.nsysu.edu.tw

Received 3 June 2014

ABSTRACT: A compact dual-antenna for the long term evolution (LTE) operation in its high band of 1710–2690 MHz is presented for the LTE tablet computer application. The dual-antenna occupies a small volume of $10 \times 45 \times 0.8 \text{ mm}^3$ and comprises two back-to-back folded loops separated by a π -shape grounded strip. Each folded loop is directly fed to generate its half-wavelength mode at about 2.6 GHz, and one arm of the π -shape grounded strip is parasitically excited to provide a quarter-wavelength resonant mode at about 1.9 GHz. The two resonant modes are formed into a wide operating band of about 1.7–2.7 GHz, which covers the desired LTE high band. Furthermore, the other arm of the π -shape grounded strip provides a resonant path to direct the excited surface currents on the device ground plane. In this case, the surface currents flowing along the top edge of the device ground plane is greatly suppressed, thereby decreasing the coupling between the two feeding ports of the dual-antenna. The dual-antenna provides acceptable isolation better than about 10 dB and good antenna efficiency better than about 55% over a wide operating band of larger than 1 GHz. This leads to acceptable envelope correlation coefficient (<0.3 for the proposed dual-antenna) obtained for the LTE high-band (1710–2690 MHz) operation. Operating principle of enhanced bandwidth and decreased coupling of the dual-antenna is described. Results of the fabricated dual-antenna are presented, and the MIMO performance of the dual-antenna is also discussed. © 2015 Wiley Periodicals, Inc. *Microwave Opt Technol Lett* 57:104–111, 2015; View this article online at wileyonlinelibrary.com. DOI 10.1002/mop.28791

Key words: mobile antennas; dual-antenna systems; tablet computer antennas; LTE antennas; wideband antennas; small-size antennas

1. INTRODUCTION

Modern mobile terminal devices are generally required to support the long term evolution (LTE) operation for fourth-generation communications. The LTE operation generally includes the low band of 698–960 MHz and the high band of 1710–2690 MHz [1]. For either the LTE low-band or high-band operation, the dual-antenna with wideband operation and wideband decoupling is required. Furthermore, owing to the limited space available in the terminal device such as the smartphone and tablet computer, the dual-antenna with a compact size is demanded for practical applications.

Interesting techniques of achieving wideband operation and decreased coupling for the dual-antenna have also been reported in the literature [2–4]. These dual-antennas show decreased coupling over a wide operating band. In [2], the technique of using a T-shape protruded ground separating two printed antennas achieves a wideband of 2.3–7.7 GHz with an isolation better than 20 dB for the laptop network card application. In [3], the use of a tree-like structure between two printed antennas achieves an isolation better than 16 dB over the wideband of 3.1–10.6 GHz. In [4], the use of a neutralization-line technique between two printed monopoles achieves an isolation better than 17 dB over the wideband of 2.4–4.2 GHz.

Recently, the wideband dual-antennas that are promising to cover the entire LTE low band [5] and LTE high band [6,7] have also been reported. In [5], the dual-antenna with a volume of $15 \times 60 \times 5 \text{ mm}^3$ in the mobile phone can have the full coverage of the entire LTE low band with a port-to-port isolation of better than about 11 dB. The wideband decoupling is achieved using an inductor-loaded neutralization line [5]. To achieve wideband decoupling for the LTE high-band (1710–2690 MHz) operation, the techniques of using grounded branches [6,7] have been applied for the wideband dual-antenna. In [6], the dual-antenna uses two grounded branches and an inverted-U-shape neutralization line and requires a clearance region of $15 \times 60 \text{ mm}^2$. The dual-antenna reports an isolation of better than 15 dB in the 1.70–2.76 GHz band. In [7], four grounded branches are used for the dual-antenna to achieve an isolation of better than 15 dB in the 1.67–2.75 GHz band. However, the dual-antenna requires a clearance region of $17 \times 60 \text{ mm}^2$.

It is noted that the wideband dual-antennas that have been reported [2–7] show a high profile (15 mm or larger), which limits their possible applications in modern mobile terminal devices. This is because the spacing or ground clearance region allowed for the embedded antennas therein is becoming very narrow, which is generally 10 mm or even smaller. In addition, it is also demanded that the antenna's occupied ground clearance be as small as possible, such that more antennas or dual-antennas can be embedded inside the mobile terminal device.

To meet such application requirements, we present in this article a compact wideband dual-antenna that can cover the entire LTE high band of 1710–2690 MHz. The proposed dual-antenna occupies a small ground clearance of $10 \times 45 \text{ mm}^2$ and is printed on a 0.8-mm thick FR4 substrate, making it promising for applications in modern slim tablet devices, such as the tablet computer. The dual-antenna comprises two back-to-back folded loops separated by a π -shape grounded strip. For each antenna, the wideband operation is obtained by two resonant modes excited, respectively, by the folded loop and one arm of the π -shape grounded strip. Also, the other arm of the π -shape grounded strips can provide a resonant path to direct the surface currents excited on the device ground plane, such that the surface currents flowing along the top edge of the device ground plane is greatly suppressed. This greatly decreases the coupling between the two feeding ports of the dual-antenna. The proposed dual-antenna has acceptable isolation better than about 10 dB and good antenna efficiency better than about 55% over a wide operating band of larger than 1 GHz. The obtained envelope correlation coefficient (ECC) is also less than 0.3 for the proposed dual-antenna for the LTE operation in the 1710–2690 MHz band, which is acceptable for practical applications [8]. Details of the dual-antenna, including the operating principle of enhanced bandwidth and decreased coupling between the two antennas thereof, are described. Measured results of the fabricated dual-antenna are presented, and its MIMO performance [9] is also discussed.

2. PROPOSED DUAL-ANTENNA

2.1. Dual-Antenna Structure

Figure 1 shows the geometry of the compact dual-antenna for the LTE tablet computer application. The dual-antenna is printed on a 0.8-mm thick FR4 substrate of size $10 \times 45 \text{ mm}^2$, relative permittivity 4.4, and loss tangent 0.024. To show the dual-antenna structure more clearly for understanding, a photo of the fabricated dual-antenna is presented in Figure 2. In the study for

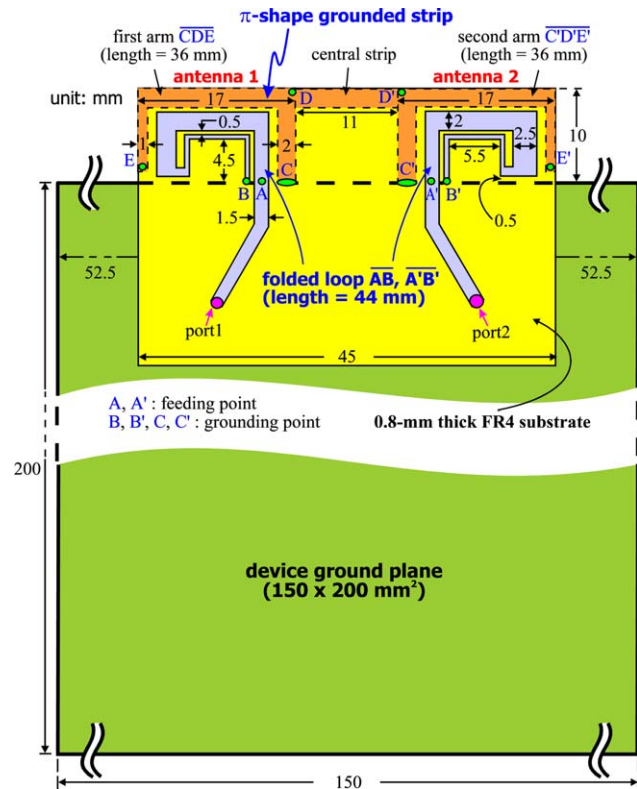


Figure 1 Geometry of the compact dual-antenna for the LTE tablet computer. [Color figure can be viewed in the online issue, which is available at wileyonlinelibrary.com]

the tablet computer application, the dual-antenna is mounted at the center of the top edge (short edge) of the device ground plane, which has a size of $200 \times 150 \text{ mm}^2$. The device ground plane size is selected to fit for a 9.7-inch tablet computer.

The two antennas (antenna 1 and 2) in the proposed dual-antenna are symmetric in structure and have same dimensions. Antenna 1 and 2 are fed through port 1 and 2, respectively. The dual-antenna is formed by two back-to-back folded loops (loop 1 and 2) and a π -shape grounded strip placed in-between. The grounded strip has a first arm (section CDE, length 36 mm), a second arm (section C'D'E', length 36 mm), and a central metal strip (section DD', length 11 mm). In this case, antenna 1 can be considered to comprise loop 1 and the first arm, while antenna 2 includes loop 2 and the second arm. Both loop 1 and 2 have a length of about 44 mm and are directly excited to generate a half-wavelength loop mode [10–12] at about 2.6 GHz. Since the loop antenna has a closed resonant path, the electric field of the loop resonant mode thereof will be weak. This property can help decrease the coupling between port 1 and 2 in the dual-antenna.

Furthermore, the π -shape grounded strip not only performs as a radiator but also serves as an isolator to enhance the isolation of the dual-antenna. When loop 1 is excited, the first arm of the π -shape grounded strip is parasitically excited to provide a quarter-wavelength resonant mode at about 1.9 GHz. The two resonant modes at about 1.9 and 2.6 GHz are formed into a wide operating band of about 1.7–2.7 GHz, which covers the desired LTE high band. At the same time, the second arm of the π -shape grounded strip and the central metal strip together can provide a resonant path to direct the excited surface currents on the device ground plane. This behavior is similar to the effect of

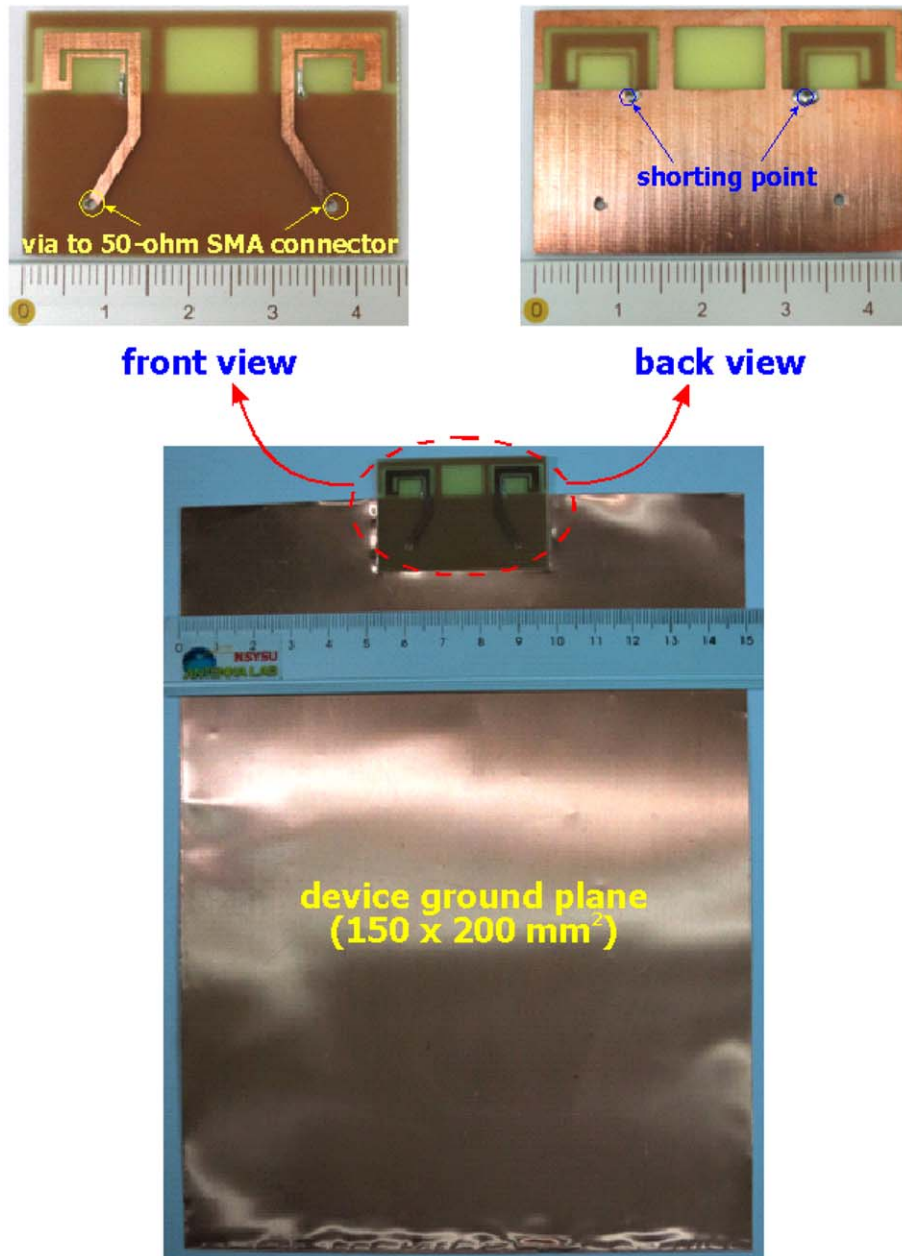


Figure 2 Photos of the fabricated dual-antenna. [Color figure can be viewed in the online issue, which is available at wileyonlinelibrary.com]

using a protruded ground for isolation enhancement [13,14]. In this case, the excited surface currents flowing along the short edge from antenna 1 to antenna 2 can be effectively suppressed. The proposed dual-antenna can hence have decreased coupling.

2.2. Operating Principle

To address the operating principle of enhanced bandwidth and decreased coupling of the dual-antenna in more detail, Figure 3 shows the simulated S -parameters for the proposed dual-antenna, the case with two folded loops only (Dual-ant1), and the case with two folded loops and the first and second arms of the π -shape grounded strip only (Dual-ant2). The simulated results are obtained using the full-wave electromagnetic field simulator HFSS version 15 [15]. The shaded frequency region in the figure indicates the desired LTE high band (1710–2690 MHz). For Dual-ant1, only one resonant mode is excited at about 2.6 GHz [see the S_{11} results in Figure 3(a)], which is con-

tributed by the folded loop, and the bandwidth is far from covering the LTE high band. Note that for the simulated results, S_{22} is the same as S_{11} and is not shown for brevity. For Dual-ant2, a new resonant mode occurs at about 1.9 GHz, which is owing to the presence of the first arm of the π -shape grounded strip. In this case, with two resonant modes excited, a wide operating band of about 1 GHz is obtained. When the central metal arm is added to form the π -shape grounded strip, the impedance matching for frequencies over the LTE high band is further enhanced. In addition, as seen in Figure 3(b), the S_{21} is decreased for the proposed dual-antenna. At 2500 MHz, compared to Dual-ant2, a decreased of 10 dB in S_{21} is seen for the proposed dual-antenna. Over the LTE high band, the S_{21} of about -10 to -13 dB is obtained for the proposed dual-antenna.

The simulated surface current distributions at 1750, 2300, and 2500 MHz for the proposed dual-antenna and Dual-ant2 are also presented in Figure 4 for comparison. Note that the excited

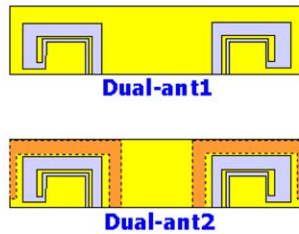
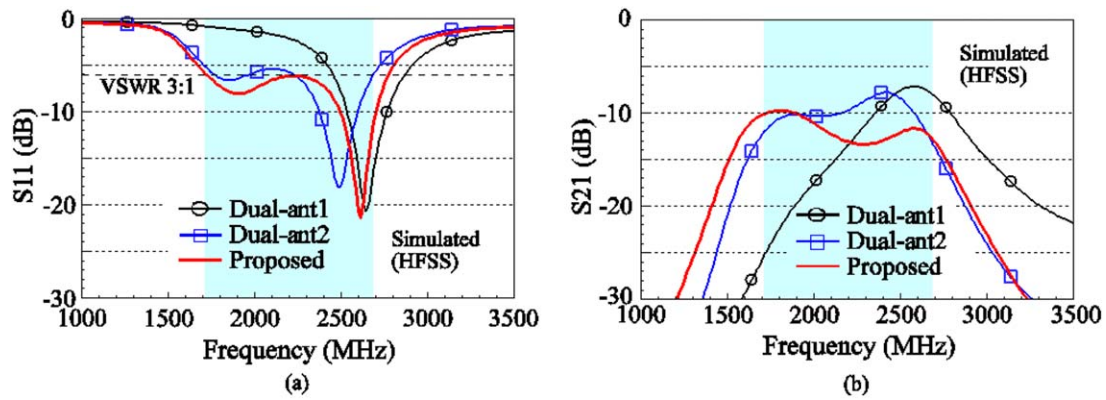


Figure 3 Simulated S parameters for the proposed dual-antenna, the case with two folded loops only (Dual-ant1), and the case with two folded loops and the first and second arms of the π -shape grounded strip only (Dual-ant2). (a) S_{11} . (b) S_{21} . [Color figure can be viewed in the online issue, which is available at wileyonlinelibrary.com]

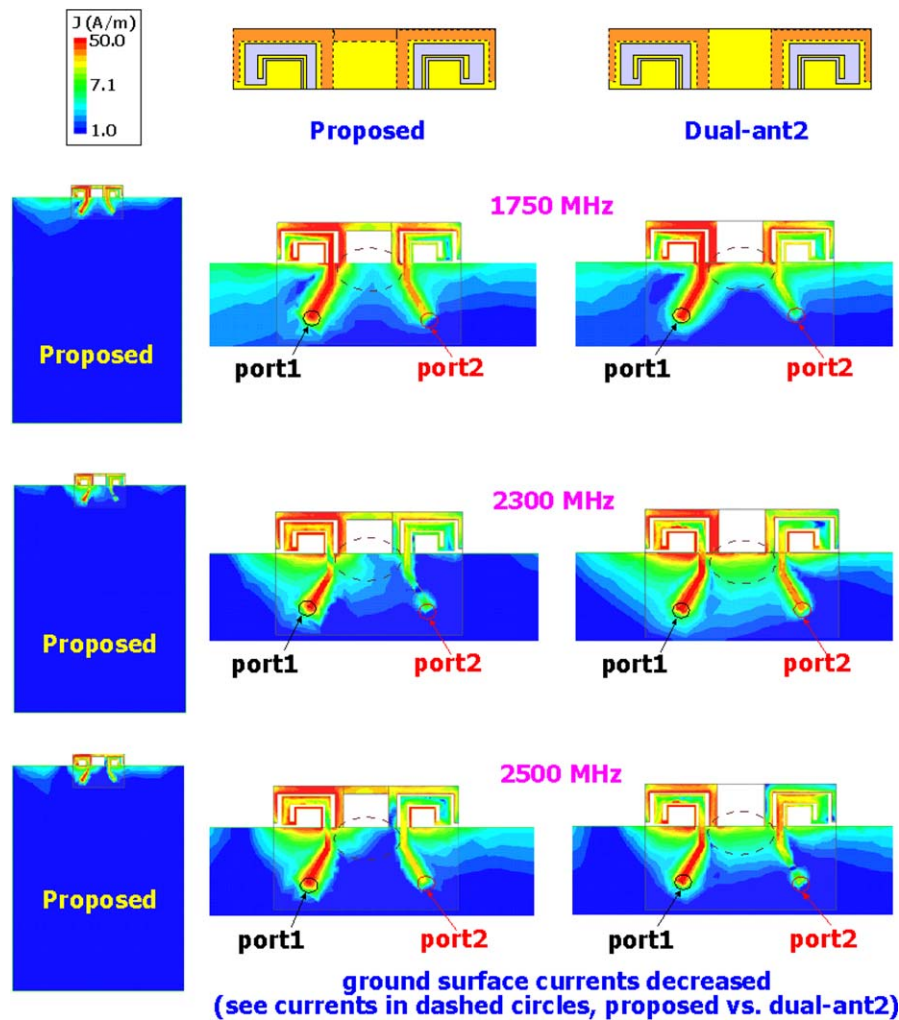


Figure 4 Simulated surface current distributions on the proposed dual-antenna and Dual-ant2. [Color figure can be viewed in the online issue, which is available at wileyonlinelibrary.com]

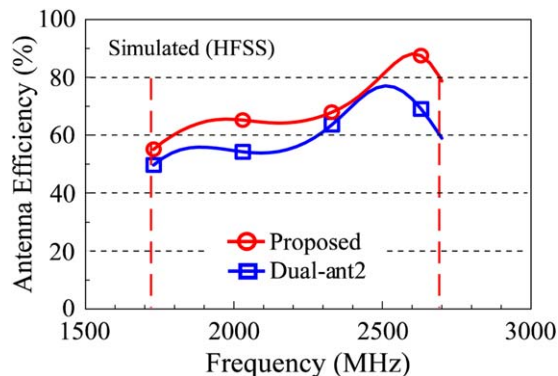


Figure 5 Simulated antenna efficiency (mismatching losses included) for the proposed dual-antenna and Dual-ant2. [Color figure can be viewed in the online issue, which is available at wileyonlinelibrary.com]

surface currents along the short edge between the two antennas are decreased. This confirms that either arm of the π -shape grounded strip and the central metal strip together can provide a resonant path to direct the excited surface currents on the device ground plane. In this case, the coupling between the two antennas can be decreased.

Figure 5 shows the simulated antenna efficiency for the proposed dual-antenna and Dual-ant2. The antenna efficiency includes the mismatching losses. It is seen that the antenna efficiency for the proposed dual-antenna is about 10% higher than that of Dual-ant2, and the antenna efficiency is about 55–88% over the LTE high band. Figure 6 shows the simulated ECC for the proposed dual-antenna and Dual-ant2. The ECC is obtained from the simulated electric-field patterns [9]. It is seen that, compared to Dual-ant2, the simulated ECC of the proposed dual-antenna is greatly decreased to be less than 0.3 over the entire LTE high band. The obtained ECC indicates that the two antennas in the proposed dual-antenna are loosely coupled, which are acceptable for practical MIMO applications.

3. EXPERIMENTAL RESULTS AND DISCUSSION

3.1. Experimental Results

The fabricated dual-antenna centered at the short edge of the device ground plane as shown in Figure 2 is tested. Figure 7 shows the measured and simulated S -parameters of the fabricated dual-antenna. Good agreement between the measurement and simulation is obtained. Over the LTE high band, the meas-

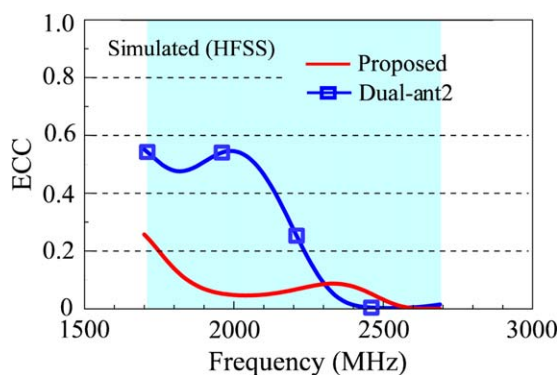


Figure 6 Simulated ECC for the proposed antenna and Dual-ant2. [Color figure can be viewed in the online issue, which is available at wileyonlinelibrary.com]

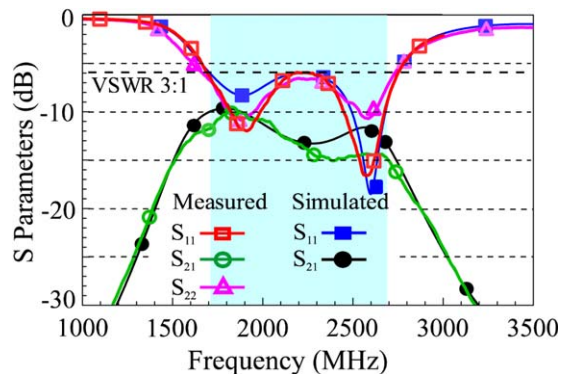


Figure 7 Measured and simulated S parameters of the fabricated dual-antenna. [Color figure can be viewed in the online issue, which is available at wileyonlinelibrary.com]

ured S_{11} is less than -6 dB (3:1 VSWR), indicating that the proposed dual-antenna can cover the LTE high-band operation. Also, within the operating band, the S_{21} is less than about -10 dB, which can lead to acceptable ECC for the MIMO operation. The calculated ECC from the measured results will be analyzed with the aid of Figure 10 later.

Figure 8 shows the measured and simulated antenna efficiencies of the fabricated dual-antenna. The experimental results are measured in a far-field anechoic chamber. The measured results for port1 and port2 excitation are presented. For the simulated antenna efficiency, as the results for port1 and port2 excitation are the same, only those for port1 excitation are shown for comparison. Results show that the measured antenna efficiencies agree with the simulated results. The slight deviations of the measured antenna efficiencies for port1 and port2 excitation may be owing to the fabrication errors and the measurement misalignment. In general, the measured antenna efficiencies for the fabricated dual-antenna are varied from about 52–84% for frequencies over the LTE high band. The obtained antenna efficiencies are acceptable for practical mobile communication applications [16,17].

Figure 9 shows the measured radiation patterns of the fabricated dual-antenna. Three frequencies at 1750, 2300, and 2500 MHz are shown. For brevity, only the results for port1 excitation are presented. At each frequency, the radiation patterns in three principal planes are plotted, and the radiation intensities in the three radiation patterns are normalized with respect to the

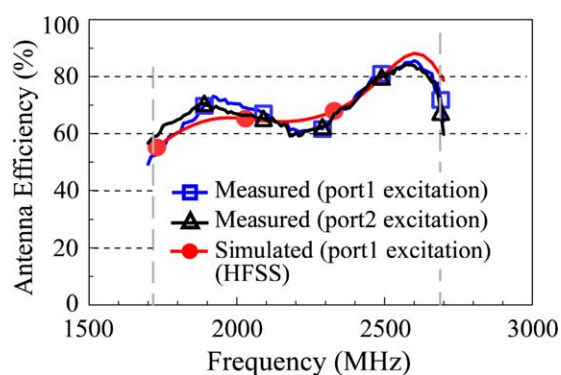


Figure 8 Measured and simulated antenna efficiencies of the fabricated dual-antenna. [Color figure can be viewed in the online issue, which is available at wileyonlinelibrary.com]

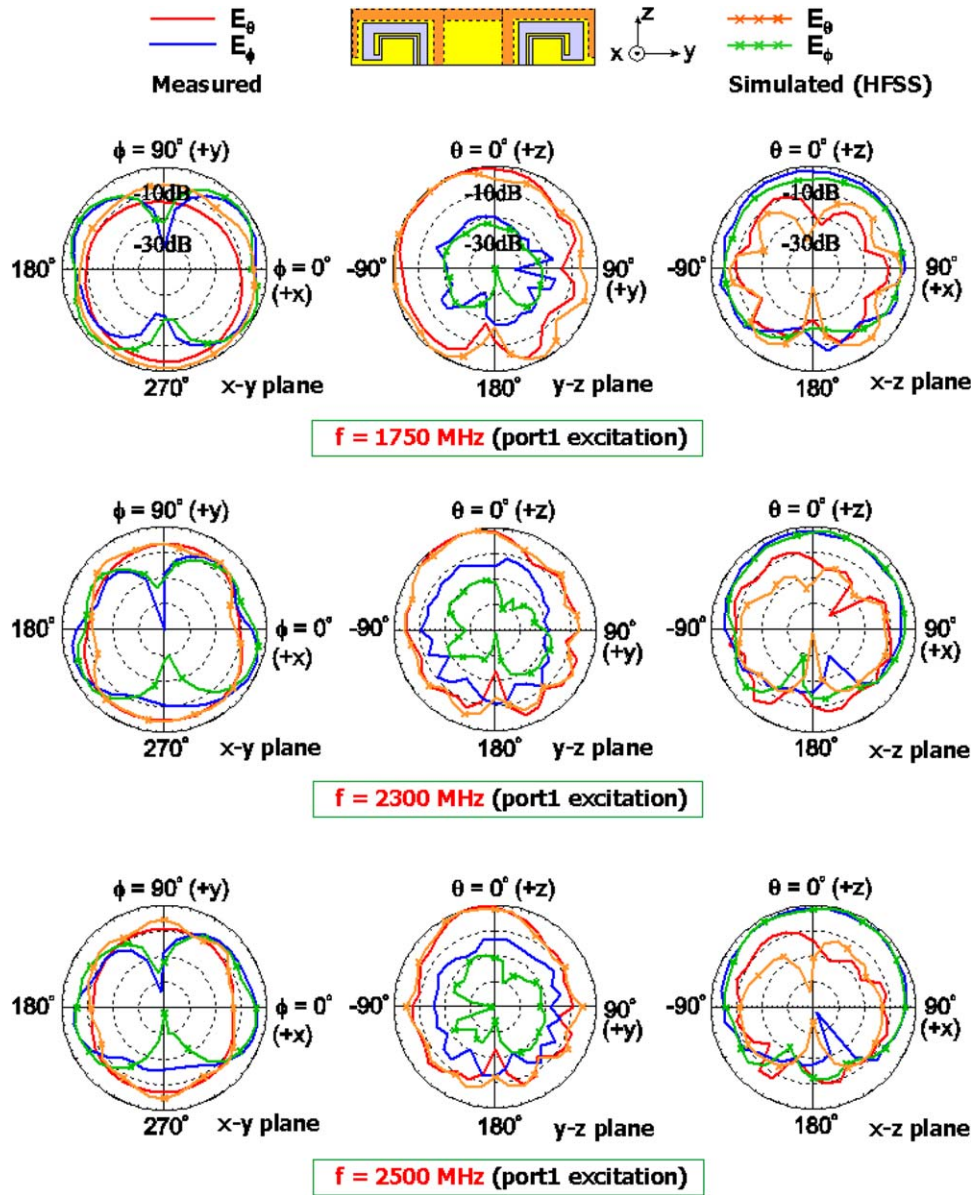


Figure 9 Measured and simulated radiation patterns of the fabricated dual-antenna. [Color figure can be viewed in the online issue, which is available at wileyonlinelibrary.com]

same maximum intensity. It is seen that in the x - y plane (azimuthal plane), the E_θ and E_ϕ radiation at three frequencies are all comparable. This is advantageous for practical applications, mainly because the wave propagation environment for mobile communication is usually complex. In the y - z plane (elevation plane parallel to the device ground plane), the radiation patterns are seen to be tilted to the $-y$ direction. This is probably because for port1 excitation, antenna 1 of the dual-antenna is excited, and antenna 1 is in the $-y$ direction with respect to the center of the short edge of the device ground plane. In the x - z plane (elevation plane perpendicular to the device ground plane), stronger radiation in the upper half-plane ($+z$ direction) is seen. This indicates that the device ground plane mainly acts as a reflector for frequencies in the LTE high band [18–20].

3.2. MIMO Performance

The ECC, mean effective gain (MEG), and channel capacity (CC) [9] are calculated to evaluate the MIMO performance of the dual-antenna. The ECC and MEG are calculated from the

measured three-dimensional electric-field patterns of antenna 1 and 2 of the fabricated dual-antenna with the assumption of uniform incident wave environment. In this case, both the angular power functions in the θ and ϕ polarizations of the incoming wave are set to $1/4\pi$ in all directions, and the cross polarization ratio of the incident wave is assumed to be 0 dB (that is, the indoor propagation environment is assumed). Figure 10 shows the simulated ECC obtained using HFSS version 15 [15] and the calculated ECC from the measured electric-field patterns of the fabricated dual-antenna. Results indicate that the calculated ECC is less than 0.3 over the entire LTE high band, which satisfies the criterion of acceptable ECC (<0.5) [8]. The simulated ECC in general agrees with the calculated ECC from the measured electric-field patterns. Some deviations between the two curves in the figure are very probably owing to slight misalignments of the antenna in the anechoic chamber during the experimental testing for the three-dimensional electric-field patterns.

Figure 11 shows the calculated MEG of antenna 1 (port1 excitation) and antenna 2 (port2 excitation) from the measured

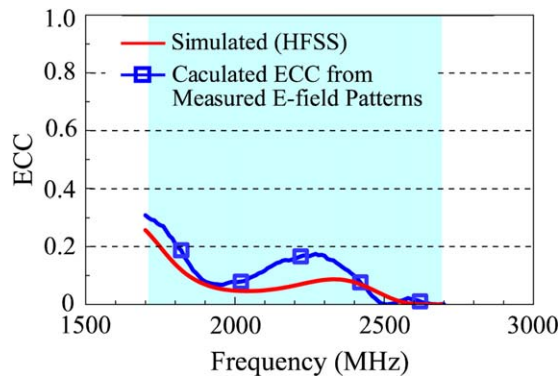


Figure 10 Comparison of simulated ECC and calculated ECC from the measured electric-field patterns of the fabricated dual-antenna. [Color figure can be viewed in the online issue, which is available at wileyonlinelibrary.com]

electric-field patterns of the fabricated dual-antenna. The MEGs for port1 and port2 excitation are varied from about -3.7 to -6.0 dBi, and the differences of MEGs are less than 0.5 dBi for frequencies over the LTE high band. The results indicate that antenna 1 and 2 have comparable MEGs, which is good for practical MIMO applications [6–9].

Ergodic CC for a 2×2 MIMO antenna system is calculated. The condition of uncorrelated transmitting antennas and identically and independently distributed (i.i.d.) channels with Rayleigh fading environment is assumed [21]. At each frequency, the capacity is averaged over 10,000 Rayleigh fading realizations with a signal-to-noise ratio of 20 dB at the mobile terminal. Figure 12 shows the ergodic channel capacities of the fabricated dual-antenna. Note that the upper limit for a single-antenna with perfect antenna efficiency (100%) is 6.25 bps/Hz, and that for a dual-antenna with perfect antenna efficiency (100%) and perfect ECC (0) is 12.5 bps/Hz. For the proposed dual-antenna with measured antenna efficiency shown in Figure 8 and calculated ECC from measured electric-field patterns shown in Figure 10, the obtained capacities are varied from 10.3 to 12.0 bps/Hz, which are much larger than the upper limit of a single-antenna and are close to that of the perfect dual-antenna. The obtained results indicate that the proposed dual-antenna is promising for MIMO applications.

4. CONCLUSION

A compact dual-antenna with a π -shape grounded strip for LTE tablet computer application has been proposed. The compact

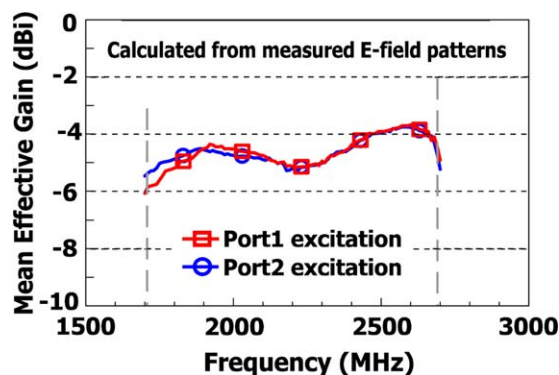


Figure 11 Calculated MEG of antenna 1 and 2 from the measured electric-field patterns of the fabricated dual-antenna. [Color figure can be viewed in the online issue, which is available at wileyonlinelibrary.com]

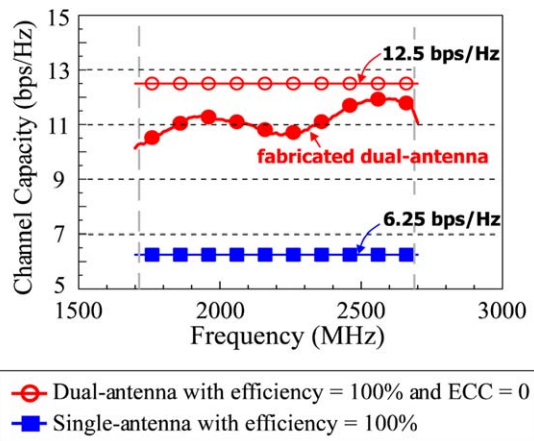


Figure 12 Ergodic channel capacities of the fabricated dual-antenna. [Color figure can be viewed in the online issue, which is available at wileyonlinelibrary.com]

structure of the dual-antenna is obtained using a π -shape grounded strip to enclose two folded loops fed by two feeding ports. The π -shape grounded strip leads to enhanced bandwidth and decreased coupling of the two antennas in the proposed dual-antenna. For enhanced bandwidth, it is obtained owing to the two arms of the π -shape grounded strip contributing additional resonant modes in the desired operating band. In this study, the dual-antenna can cover the LTE high band of 1710–2690 MHz with a small size of $10 \times 45 \times 0.8$ mm³. For decreased coupling, it is because the π -shape grounded strip can effectively detour the surface currents excited on the device ground plane. This leads to acceptable isolation obtained for the dual-antenna, although the two antennas thereof are very closely spaced. Acceptable ECCs and MEGs of the dual-antenna in the LTE high band have also been obtained. The calculated ergodic channel capacities are about 10.3–12.0 bps/Hz with the assumption of uniform incident wave environment and i.i.d. channels with Rayleigh fading environments. With the compact size and acceptable MIMO performance, the proposed dual-antenna is promising for the tablet computer application in the LTE high band.

REFERENCES

1. LTE Frequency Bands & Spectrum Allocations-a summary: tables of the LTE frequency band spectrum allocations for 3G & 4G LTE - TDD and FDD. Available at: <http://www.radio-electronics.com/>.
2. K.L. Wong, S.W. Su, and Y.L. Kuo, A printed ultra-wideband diversity monopole antenna, *Microwave Opt Technol Lett* 38 (2003), 257–259.
3. S. Zhang, Z. Ying, J. Xiong, and S. He, Ultrawideband MIMO/diversity antennas with a three-like structure to enhance wideband isolation, *IEEE Antennas Wireless Propag Lett* 8 (2009), 1279–1282.
4. C.H. See, R.A. Abd-Alhameed, Z.Z. Abidin, N.J. McEwan, and P.S. Excell, Wideband printed MIMO/diversity monopole antenna for WiFi/WiMAX applications, *IEEE Trans Antennas Propag* 60 (2012), 2028–2035.
5. A. Cihangir, F. Ferrero, G. Jacquemod, P. Brachat, and C. Luxey, Neutralized coupling elements for MIMO operation in 4G mobile terminals, *IEEE Antennas Propag Lett* 13 (2014), 141–144.
6. Y. Wang and Z. Du, A wideband printed dual-antenna system with a novel neutralization line for mobile terminals, *IEEE Antennas Wireless Propag Lett* 12 (2013), 1428–1431.
7. Y. Wang and Z. Du, A printed dual-antenna system operating in the GSM1800/GSM1900/UMTS/LTE2300/LTE2500/2.4-GHz WLAN bands for mobile terminals, *IEEE Antennas Wireless Propag Lett* 13 (2014), 233–236.

8. Y.L. Ban, S. Yang, Z. Chen, K. Kang, and J.L.W. Li, Decoupled planar WWAN antennas with T-shaped protruded ground for smartphone applications, *IEEE Antennas Wireless Propag Lett* 13 (2014), 483–486.
9. M.S. Sharawi, Printed multi-band MIMO antenna systems and their performance metrics, *IEEE Antennas and Propag Mag* 55 (2013), 218–232.
10. Y.W. Chi and K.L. Wong, Compact multiband folded loop chip antenna for small-size mobile phone, *IEEE Trans Antennas Propag* 56 (2008), 3797–3803.
11. W.Y. Li and K.L. Wong, Surface-mount loop antenna for AMPS/GSM/DCS/PCS operation in the PDA phone, *Microwave Opt Technol Lett* 49 (2007), 2250–2254.
12. Y.W. Chi and K.L. Wong, Quarter-wavelength printed loop antenna with an internal printed matching circuit for GSM/DCS/PCS/UMTS operation in the mobile phone, *IEEE Trans Antennas Propag* 57 (2009), 2541–2547.
13. K.L. Wong, T.W. Kang, and M.F. Tu, Internal mobile phone antenna array for LTE/WWAN and LTE MIMO operations, *Microwave Opt Technol Lett* 53 (2011), 1569–1573.
14. K.L. Wong, P.W. Lin, and H.J. Hsu, Decoupled WWAN/LTE antennas with an isolation ring strip embedded there between for smartphone application, *Microwave Opt Technol Lett* 55 (2013), 1470–1476.
15. ANSYS HFSS. Ansoft Corp., Pittsburgh, PA, Available at: <http://www.ansys.com/products/hf/hfss/>.
16. K.L. Wong and M.T. Chen, Small-size LTE/WWAN printed loop antenna with an inductively coupled branch strip for bandwidth enhancement in the tablet computer, *IEEE Trans Antennas Propag* 61 (2013), 6144–6151.
17. K.L. Wong and L.Y. Chen, Small-size LTE/WWAN tablet device antenna with two hybrid feeds, *IEEE Trans Antennas Propag* 62 (2014), 2926–2934.
18. K.L. Wong, H.J. Jiang, and T.W. Weng, Small-size planar LTE/WWAN antenna and antenna array formed by the same for tablet computer application, *Microwave Opt Technol Lett* 55 (2013), 1928–1934.
19. K.L. Wong and T.W. Weng, Small-size triple-wideband LTE/WWAN tablet device antenna, *IEEE Antennas Wireless Propag Lett* 12 (2013), 1516–1519.
20. P.W. Lin and K.L. Wong, Low-profile multibranch monopole antenna with integrated matching circuit for LTE/WWAN/WLAN operation in the tablet computer, *Microwave Opt Technol Lett* 56 (2014), 1662–1666.
21. A.A. Al-Hadi, J. Ilvonen, R. Valkonen, and V. Viikari, Eight-element antenna array for diversity and MIMO mobile terminal in LTE 3500 MHz band, *Microwave Opt Technol Lett* 56 (2014), 1323–1327.

© 2015 Wiley Periodicals, Inc.

A COMPACT NOVEL CPW-FED ANTENNA WITH SQUARE SPIRAL-PATCH FOR MULTIBAND APPLICATIONS

Payam Beigi,¹ Javad Nourinia,² Yashar Zehforoosh,³ and Bahman Mohammadi²

¹Department of Electrical Engineering, Science and Research Branch Islamic Azad University, West Azarbaijan, Iran; Corresponding author: payam.beigi@yahoo.com

²Department of Electrical Engineering, Urmia University, Urmia, Iran

³Department of Electrical Engineering, Urmia Branch, Islamic Azad University, Urmia, Iran

Received 9 June 2014

ABSTRACT: A compact novel coplanar waveguide-fed antenna with square spiral-patch for multiband applications is presented. The antenna consists of a square-spiral patch with two L-shape strips. With subjoin square spiral the number of frequency resonance is increasing. Also by introducing two L-shaped strips in the inside of square spiral, much wider impedance bandwidth can be produced, especially at the higher bands. The operating frequencies of the proposed antenna are 2.62/3.40/4.42/5.92/8.32 GHz. Some key parameters affecting the antenna perform-

ance have been analyzed using computer simulations. To validate the simulation results, the prototypes of the proposed antenna are fabricated on an inexpensive FR-4 substrate and tested. Good radiation characteristics of the proposed antenna have been obtained. The simulated and measured results are in good agreement. © 2015 Wiley Periodicals, Inc. *Microwave Opt Technol Lett* 57:111–115, 2015; View this article online at wileyonlinelibrary.com. DOI 10.1002/mop.28783

Key words: coplanar waveguide-fed antenna; multiband applications; square spiral-patch

1. INTRODUCTION

In modern wireless communication systems, multiband antenna has been playing a very important role for wireless service requirements. Wireless local area network (WLAN) and worldwide interoperability for microwave access (WiMAX) have been widely applied in mobile devices, such as handheld computers and intelligent phones. These two techniques have been widely recognized as a viable, cost-effective, and high-speed data connectivity solution, enabling user mobility. In practice, IEEE 802.11 WLAN standards consist of 2.4-GHz (2.4–2.484 GHz), 5.2-GHz (5.15–5.35 GHz), and 5.8-GHz (5.725–5.875 GHz) frequency bands. WiMAX standards consist of 3.5-GHz (3.3–3.6 GHz) and 5.5-GHz (5.25–5.85 GHz) frequency bands [1,2]. A lot of effort has been put into designing new antennas which can satisfy the requirements of modern communication systems. As a result of accelerating growth of wireless technology, there has been a vast body of literature introducing novel antennas for dual- and multiband applications and systems [1–12].

In this context, many articles have been introduced. For instance in [1], a hybrid ring fractal printed monopole antenna with a very compact size and good impedance and radiation characteristics for WLAN/WiMAX applications presented. [4] Proposes an antenna using coplanar waveguide (CPW)-fed tri-band planar monopole antenna for WLAN/WiMAX applications. The main aim of the article is to obtain an antenna with reduced size. In [6], a triple-band planar antenna with a compact radiator is proposed for 2.3/3.5/5.5 GHz WiMAX and 5.2/5.8 GHz WLAN applications simultaneously. The proposed antenna consists of an inverted-L-shaped radiating element and a parasitic element in the ground plane to generate three resonant modes for triple-band operations. Using two F-shaped slits into the rectangular patch in [10] a novel CPW-fed monopole antenna is introduced for WLAN and WiMAX applications. In [13], a novel type of printed and doubled-sided dipole antenna for multiband operation is presented; the proposed antenna is fed by a 50-Ω coaxial cable through a microstrip-to-twinline tapered transition. Moreover, other strategies to improve the impedance bandwidth which do involve a modification of the geometry of the planar antenna have been investigated [7–9,12].

In this article, compact novel CPW-fed antenna with square spiral-patch for multiband applications has been presented. The antenna consists of a square-spiral patch with two L-shaped strips. With subjoin square spiral the number of frequency resonance is increasing. Also by introducing two L-shape strips in the inside of square spiral, much wider impedance bandwidth can be produced, especially at the higher bands. With simple structure and small size, the measured results show that the proposed antenna has 10-dB impedance bandwidths of 474 MHz (2.335–2.809 GHz), 214 MHz (3.362–3.540 GHz), 164 MHz (4.324–4.488 GHz), 176 MHz (5.811–5.987 GHz), and 492 MHz (7.994–8.486 GHz) to cover all the 2.4/5.2/5.8-GHz WLAN and the 3.5/5.5-GHz WiMAX bands, and good omnidirectional radiation characteristics are obtained over the operating bands.